CEAS Space J (2016) 8:229–236
DOI 10.1007/s12567-016-0118-4

ORIGINAL PAPER

Numerical and experimental analysis of spallation phenomena

Alexandre Martin[1] · Sean C. C. Bailey[1] · Francesco Panerai[1] · Raghava S. C. Davuluri[1] · Huaibao Zhang[1] · Alexander R. Vazsonyi[1] · Zachary S. Lippay[1] · Nagi N. Mansour[2] · Jennifer A. Inman[3] · Brett F. Bathel[3] · Scott C. Splinter[3] · Paul M. Danehy[3]

Received: 22 July 2015 / Revised: 16 April 2016 / Accepted: 17 April 2016 / Published online: 23 May 2016

Abstract The spallation phenomenon was studied through numerical analysis using a coupled Lagrangian particle tracking code and a hypersonic aerothermodynamics computational fluid dynamics solver. The results show that carbon emission from spalled particles results in a significant modification of the gas composition of the post-shock layer. Results from a test campaign at the NASA Langley HYMETS facility are presented. Using an automated image processing of short exposure images, two-dimensional velocity vectors of the spalled particles were calculated. In a 30-s test at 100 W/cm^2 of cold-wall heat flux, more than 722 particles were detected, with an average velocity of 110 m/s.

Keywords Ablation · Spallation · Arcjet · Thermal protection system

1 Introduction

Low-density ablators are one of the preferred classes of materials for protecting space vehicles during atmospheric entry. Through various physical processes [1–6] such as near-surface oxidation, pyrolysis chemical reaction, vaporization, and other decomposition processes, these materials reduce the amount of heat being conducted to the surface of the vehicle. These beneficial processes usually fall under the umbrella term "ablation". The spallation phenomenon [7, 8] also belongs in this category; however, unlike the other processes involved in ablation, spallation is generally regarded as undesirable.

Spallation is typically described as the ejection of solid particles off the surface of the material. Those particles are then convected away in the flow field. The exact nature of this phenomenon is unclear, although it is likely to be caused by mechanical erosion of the fibrous surface—weakened by oxidative decomposition—combined with the shear stresses introduced by the fluid flow. Soot formation from the pyrolysis gas is also a potential cause of spalled particles. For high-density materials, the high gas pressure in closed cavities within the material can also lead to spallation.

The aerodynamic heating rates of entry vehicles may be affected by spallation through various mechanisms. For instance, the solid particles ejected from the surface can modify the near-surface chemical processes and flow field. Mechanical erosion can lead to an irregular surface, and in turn, to an augmented surface roughness. Such a modification of the surface, as well as the presence of particles in the boundary layer, could potentially trigger transition from laminar to turbulent flow. Finally, mechanical erosion results in an enhanced surface recession, thereby reducing the effectiveness of the thermal protection system (TPS).

Analysis performed on experimental results from the TPS of the Pioneer-Venus [9] and the Galileo Probes [10–12] identified spallation as the source of discrepancies between measured and predicted temperature profiles, as well as heating and ablation rates. Spectroscopic

This paper is based on a presentation at the 8th European Symposium on Aerothermodynamics for Space Vehicles, March 2–6, 2015, Lisbon, Portugal.

✉ Alexandre Martin
alexandre.martin@uky.edu

[1] University of Kentucky, Lexington, KY 40506, USA

[2] NASA Ames Research Center, Moffett Field, CA 94035, USA

[3] NASA Langley Research Center, Hampton, VA 23681, USA

measurements performed on ablative test pieces [13, 14] have also revealed CN and C emission spectra in the inviscid region. The source was attributed to spallation material from the surface; spalled particles were identified as the only mechanism capable of introducing carbon upstream of the shock.

Following these results, numerical models [13, 15–17] were developed to compute the trajectory of the particles. However, some models considered particles with constant mass and the remaining assumed sublimation as the only chemical process of the particles present. Since the particles travel through a weakly ionized flow, they tend to react with the chemical species in the flow, leaving behind product traces in the shock layer, which is not accounted for in these models. Material response codes, for example, as used by NASA to design TPS, incorporate spallation simply through the introduction of an empirically determined parameter [18]. Therefore, there is a need to better understand and model the spallation phenomenon, including its source and impact on TPS performance.

To further investigate spallation effects, a Lagrangian particle tracking code was developed. This code computes the dynamics of spalled particles as they travel through a flow field. The code uses a finite-rate chemistry model to predict the chemical interactions of the particles with the flow field. This particle tracking code can then be dynamically coupled to a computational fluid dynamics (CFD) solver which models the time-accurate hypersonic flow field around ablative samples. An analysis performed using this coupled approach is presented here.

To support the spallation modeling effort, an experimental investigation was performed at the NASA Langley Hypersonic Materials Environmental Test System (HYMETS) facility [19]. HYMETS is a 400 kW arcjet that can simulate hypersonic flight and Earth or Martian entry conditions. High-speed imagery was used to capture spalled particles ejecting from FiberForm® and PICA test samples at target heat flux conditions of 100, 200, and 400 W/cm^2. From these data, measurements of particle velocity and trajectory were obtained. An initial assessment of the data for one FiberForm® sample is presented here.

2 Numerical simulations

The flow field solutions used to predict the trajectories of spalled particles following ejection from the surface were obtained using the hypersonic CFD code KATS—Kentucky Aerothermodynamics and Thermal-response Solver [20, 21]. KATS is a three-dimensional laminar Navier–Stokes solver that computes flow fields in thermochemical nonequilibrium in the continuum regime. A two-temperature model [22] is used to account for thermal nonequilibrium in the hypersonic flow field, where a single temperature T_{tr} is used to describe translational and rotational energy modes, and another one, T_{ve}, is used to describe vibrational, electronic and electron translational energy modes.

The individual species viscosity model used to compute the diffusive fluxes was obtained using the Blottner curve fits [23]. Euken's relations [24] were used to account for species thermal conductivity. The mixture transport properties are approximated using Wilke's semi-empirical mixing rule. The standard 5-reaction air model (N_2, O_2, N, O, NO) was used to account for the reacting flow, as well as calculate the initial solution for the flow field. More information about all of these models can be found in [25].

The spallation code used for this analysis models the dynamics of individual particles ejected from the surface of a test article, using a steady-state flow field solution as an initial condition. The code uses the flow field information to determine the trajectory of the particle. The following assumptions are used to derive the governing equations:

1. The spalled particles are spherical.
2. The spalled particles are made of graphite.
3. Heat and mass transfer rates are uniform over the surface of the particle.
4. Thermophysical properties of the particle are assumed to be uniform over the entire particle.

Graphite is chosen since charred PICA is considered to be carbon, and that thermochemical properties of graphite are available in the literature. A Lagrangian formulation is employed to compute the projected path of the spalled particle. The corresponding governing equations are

$$\frac{\partial}{\partial t}\begin{pmatrix} m_p \\ m_p \mathbf{u}_p \\ m_p E_p \end{pmatrix} = \begin{pmatrix} -\dot{m}_{\mathrm{C/CO}} - \dot{m}_{\mathrm{C/CN}} - \dot{m}_{\mathrm{C/sub}} \\ \mathbf{F_D} \\ \dot{q}_{\mathrm{conv}} + p_{\mathrm{drag}} - \dot{q}_{\mathrm{rad}} + \dot{q}_{\mathrm{rxn}} \end{pmatrix}. \tag{1}$$

In the left-hand side, m_p, $\mathbf{u}_p$ and E_p are, respectively, the mass, the velocity vector and the energy of the spalled particle. In the right-hand side, $\mathbf{F}_D$, $\dot{q}_{\mathrm{conv}}$, p_{drag}, $\dot{q}_{\mathrm{rad}}$ and $\dot{q}_{\mathrm{rxn}}$ are, respectively, the drag force, the convective heating, the power loss caused by drag, the re-radiative heating and the chemical energy term.

As they travel in the flow field, the particles chemically react with the flow. As the particles lose mass, their radius is reduced. The gas/particle interaction is modeled using a finite-rate chemistry model [26, 27] that accounts for three types of heterogeneous reactions: oxidation, nitridation, and sublimation [28–31]. The three types are, respectively, represented in Eq. (1) by the mass source terms $\dot{m}_{\mathrm{C/CO}}$, $\dot{m}_{\mathrm{C/CN}}$ and $\dot{m}_{\mathrm{C/sub}}$. The complete reaction mechanism is provided in Table 1. This spallation model and coupling strategy have been extensively verified; more details are given in Ref. [29].

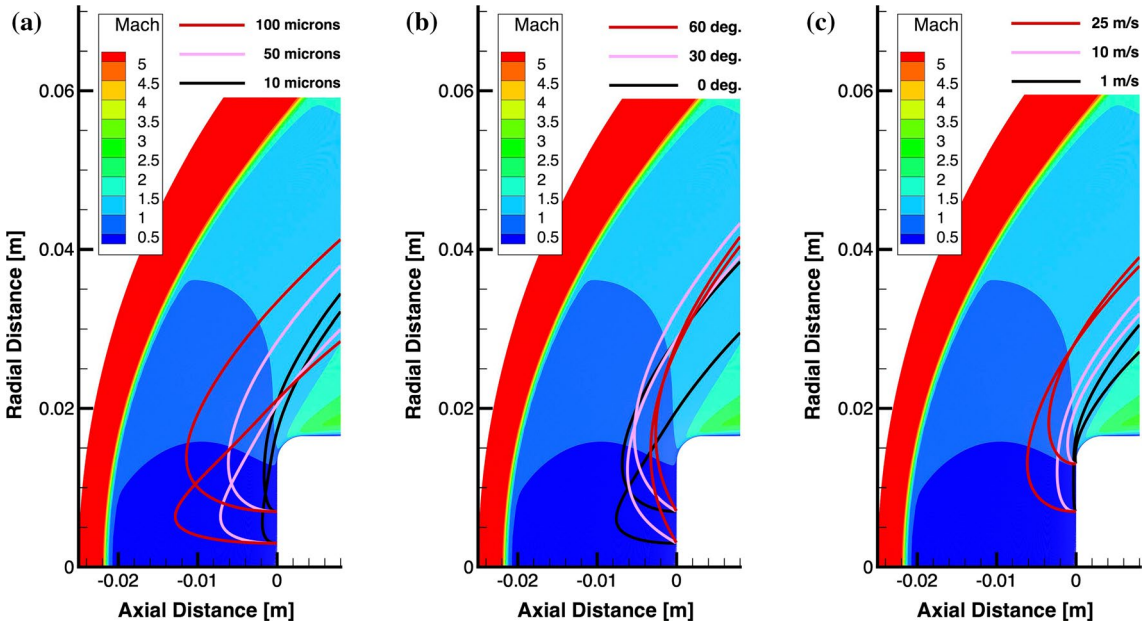

Fig. 1 Particle trajectories as a result of the study for the ejection parameters of spalled particle in a Mach 5 argon flow

Table 1 Surface chemistry model used to calculate the erosion of the spalled particles in the flow field

Reactions	Type
$C(s) + O \rightarrow CO$	Oxidation
$2C(s) + O_2 \rightarrow 2CO$	Oxidation
$C(s) + N \rightarrow CN$	Nitridation
$C(s) \rightarrow C$	Sublimation
$2C(s) \rightarrow C_2$	Sublimation
$3C(s) \rightarrow C_3$	Sublimation

Table 2 Free stream and wall properties of the Mach 5 argon flow

ρ_∞ [kg/m^3]	U_∞ [m/s]	T_{tr} [K]	T_{ve} [K]	T_w [K]
3.45×10^{-3}	3860	1470	1470	500

The test case considered here consists of a Mach 5 high-enthalpy axisymmetric flow over a cylindrical solid sample with uniform free stream flow in the direction of the cylinder axis. The sample has a diameter of 3.30 cm, an axial length of 0.82 cm, and a radius of curvature at the edge of 0.32 cm. These parameters are representative of typical test conditions achieved in the HYMETS facility [19, 32].

First, a parametric study was performed to evaluate the effects of the ejection conditions (ejection velocity, particle size and ejection angle) on the trajectory of the particle [29]. For the flow field, a Mach 5 argon flow was used, with flow conditions listed in Table 2.

In the table, T_w refers to the temperature at the surface of the sample. Argon was chosen as it simplifies the flow field solution, and allows the particle to travel the flow field without reacting. As can be seen in Fig. 1a–c, changing the ejection conditions considerably changes the trajectory of the particle. Therefore, if trajectories are measured experimentally, they could provide valuable insights about the ejection conditions.

Next, to allow evaluation of the effects of a spalled particle interacting with a flow field upstream of a test article, the spallation code was loosely coupled with KATS. The coupling procedure was performed by initially computing a steady-state solution for the flow field environment using the CFD solver. The spallation code then used the flow field data to calculate the source terms along the path of the particle. These source terms were added to the CFD code [33, 34], thus making the flow transient. To ensure time accuracy of the solution, the Courant–Friedrichs–Lewy (CFL) number was limited to be less than 1.

For this specific case, a Mach 5 air flow field was used, with conditions listed in Table 3. In this table, Y_i represents the mass faction of individual species i. For this simulation, a 30-μm carbon particle was ejected normal to the surface, 5 mm from the stagnation point, at a velocity of 90 m/s. The simulation took place over a physical time of 0.7 ms. In this work, the coupling was limited to the mass equations, and the results presented in Fig. 2 denote the concentration of total carbon products. In Fig. 2a, the entire trajectory of the particle is shown over the temperature field. Figure 2b denotes the simulation at 0.17 ms of particle travel. It can be observed that the particle tends to release

Table 3 Free stream temperature and wall properties of the Mach 5 air flow

ρ_∞ [kg/m^3]	U_∞ [m/s]	T_{tr} [K]	T_{ve} [K]	T_w [K]	Y_{Ar}	Y_{N_2}	Y_{O_2}	Y_{NO}	Y_N	Y_O
1.46×10^{-3}	3163	896	896	600	0.0704	0.7178	0.0613	0.0469	0.0000	0.1036

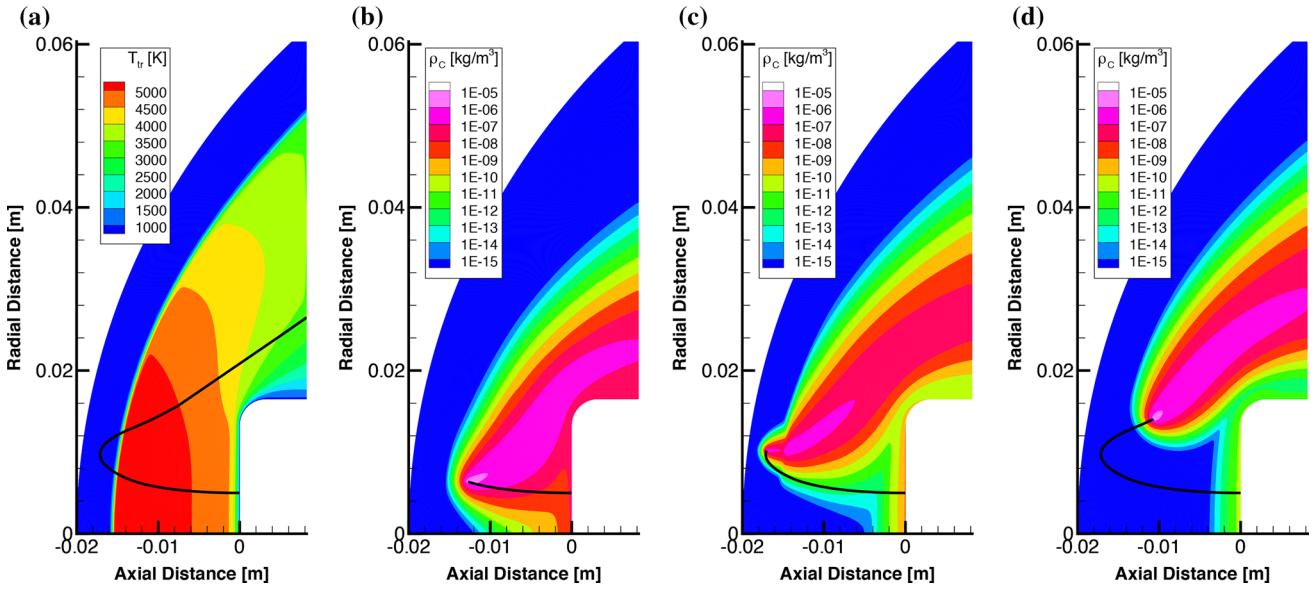

Fig. 2 Temperature, trajectory and density of the carbon species emitted from a 30-μm spalled particle ejected at 90 m/s in a Mach 5 air flow

a large amount of carbon vapor soon after ejection, due to the high concentrations of atomic oxygen and nitrogen near the wall. After 0.35 ms of travel, the particle reaches the upstream region of the shock as illustrated in Fig. 2c. The concentration of carbon vapor released decreases because of the absence of atomic species. The major contribution of carbon vapor in this region is due to particle sublimation and oxidation with molecular oxygen. The concentration of carbon vapor increases as the particle enters the shock as shown in Fig. 2d. After 0.53 ms of travel, the particle undergoes all the reactions, and the carbon concentration increases as it moves through the computational domain. It is clear from this analysis that these carbon species would react with the incoming flow, and that additional species such as CN could be created. These observations reinforce the hypothesis that spalled particles could be responsible for a previously unexplained strong spectroscopic signature observed in some arcjet test data upstream of the sample [13, 14, 35, 36].

3 Experiment

A series of tests were performed at the HYMETS facility at the NASA Langley Research Center to assess the feasibility of identifying and tracking spalled particles ejected from TPS materials. As opposed to large-scale arcjet wind tunnels, HYMETS can be operated by a minimal staff, can be run for a long period, and has essentially no downtime between runs. Hence, it is ideal for exploratory studies such as those of the present research effort. Moreover, the facility is equipped with numerous optical ports which allow the possibility of complex diagnostics and image capturing [19].

As previously noted, the purpose of the present test campaign was to confirm the presence of spalled particles for different test articles throughout a range of flow conditions. During these tests, the facility was equipped with the following:

- four high-speed cameras for particle detection at different view angles, two of them linked for stereoscopic measurements,
- an infrared camera,
- a two-color single-point pyrometer for surface temperature measurements,
- three intrusive probes for flow calibration,
- three thermocouples at the back face of each sample.

A total of ten samples of PICA [37] and FiberForm® were tested in air plasma, under three cold-wall heat flux conditions (100, 200 and 400 W/cm^2). All samples had a diameter of 3.30 cm, and a height of 2.54 cm, which included a 0.38-cm LI-2200 collar for some samples. In addition, three graphite, and three LI-2200 samples were

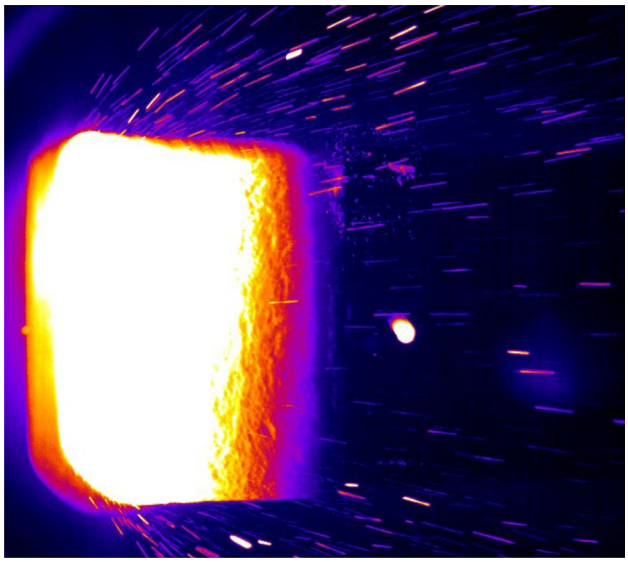

Fig. 3 Composite image of a FiberForm® sample subjected to a 400 W/cm^2 heat flux

tested under the same heat fluxes. The following section presents measurements of spalling particles using short exposure imaging, leaving a thorough documentation of the test campaign measurements to future publications.

Figure 3 is a composite image compiled during a 30-s test at 400 W/cm^2 on a FiberForm® sample. The composite image is constructed using the maximum value of the intensity at each pixel during the run. Approximately, 900 images were used, taken at a frame rate of 30 Hz with an exposure time of 25 µs. They were obtained using a 12-bit monochrome pco.dimax HD CMOS camera, cropped down to 672×608 pixels from the 1920×1080 full sensor array to reduce file size. As can be seen, numerous spalled particles were observed being ejected from the samples (note that the bright circular spot near the center of the image is not a spalled particle, but rather the head of the cylindrical pin used to secure the sample to the sting). The same observation was made at flows with lower cold-wall heat flux conditions. Spallation was systematically observed during all tests of FiberForm® and PICA samples. The graphite and LI-2200 samples, however, showed no evidence of spallation.

To provide a quantitative evaluation of the spalled particle behavior, data were analyzed from an IDT MotionXtra N-4S1, 1016×1016, 10-bit monochrome camera located orthogonally to the sample and imaging an xy-plane with x along the sample axis and y in the sample's radial direction. The test case presented here is for a FiberForm® sample subjected to a 200 W/cm^2 heat flux for 30 s. Sample surface temperature, as measured by the pyrometer, reached 2300 K during an initial 5 s transient, then increased gradually to 2400 K over the remaining 25 s of the experiment. The camera was set to double-exposure mode with the first exposure of 30 µs, followed 100 ns later by a second exposure of approximately 470 µs. Due to limitations in the onboard memory of the camera, both exposures were acquired at a sampling frequency of only 15 Hz. This ensured that images were acquired for the entire duration of the 30 s placement of the sample within the arcjet. As a result, 946 images were acquired over 31.5 s, with 473 images acquired at each exposure duration. It should be noted that only the first exposure was analyzed, with analysis of the second exposure left for future work. A single, unprocessed image is shown in Fig. 4a. A small particle trace can be seen downstream of the leading edge underneath the sample, and at least one other lower intensity particle is evident at the bottom of the image.

To analyze the image, a processing scheme was developed to isolate and enhance the particles. The first step in this process consists of subtracting the background information obtained by averaging the three consecutive images centered on the image of interest. This subtraction did not completely remove all of the radiated light emitted from the front of the sample and, therefore, pixels within this region were ignored for further processing. An amplified version of the background subtracted image is shown in Fig. 4b and multiple spalled particles are clearly observed in this single 30 µs exposure, with at least four being clearly evident and shadows of other possible particles evident as well.

Next, the image intensity was amplified by a factor of 10 and a 4×4 pixel^2 Gaussian filter applied to reduce the intensity of background noise. Using a pixel intensity threshold, the remaining pixels were identified and flagged as belonging to spalled particles. Although removing much of the background noise and residual intensity around the front face, this thresholding step also eliminated many of the lower intensity particles.

Finally, an algorithm was implemented which identified coherent groups of neighboring thresholded pixels using a 10×10 pixel^2 moving window. Each discrete group was recorded and assumed to belong to a single spalled particle. Groups containing fewer than 50 pixels were then assumed to either correspond to noise or to signals too weak to provide reliable information. Approximately, half the particles were rejected by this step. This process was fully automated, and the final results corresponding to Fig. 4a are shown in Fig. 4c. Note that many of the particles which can be observed in Fig. 4b had too low intensity to exceed the intensity threshold. In addition, one pixel grouping did not contain enough particles for further processing. Thus, this process will bias towards selection of hotter and larger particles which emit more light.

Using this process, more than 1673 discrete pixel groupings were identified over the 473 images obtained during a single run and 722 of those groupings positively identified

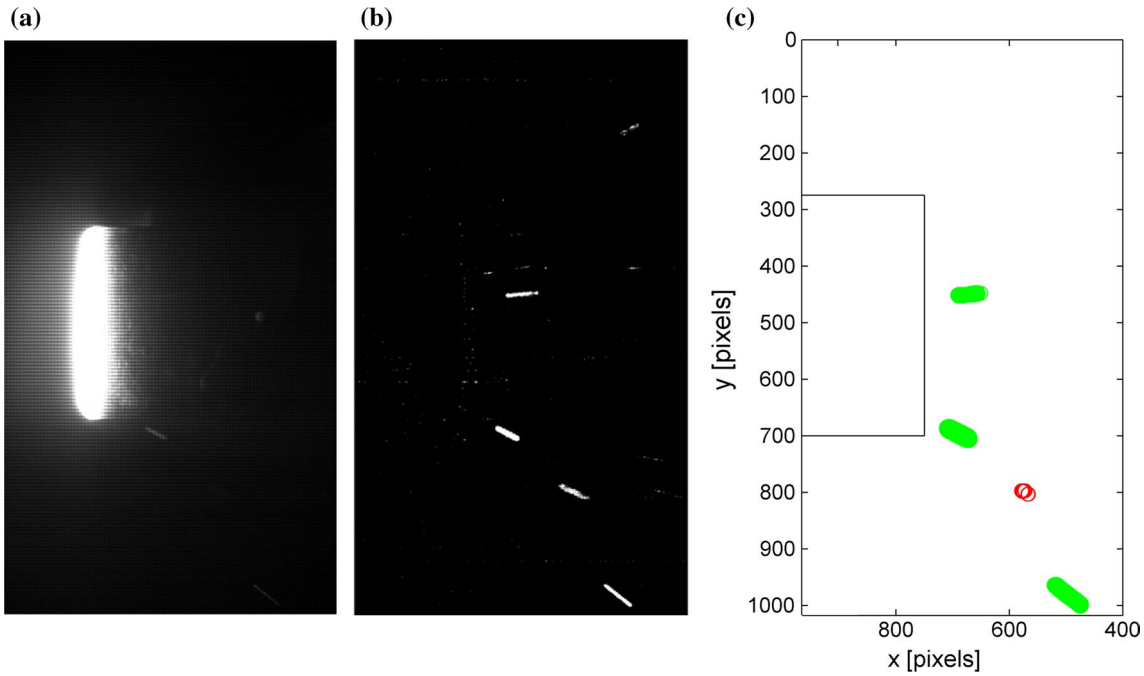

Fig. 4 FiberForm sample subjected to a 200 W/cm^2 heat flux, 12 s after introduction to arcjet. Flow from *left* to *right*. Processed image in **b** has been amplified 100× for presentation. *Black box* in **c** indicates region ignored during particle identification with three particles selected for further analysis identified in *green*

as particles. These 722 pixel groupings were then processed to estimate their velocity in the plane of the camera (here referred to as the in-plane velocity). This was done by fitting a linear line segment to the pixel groups to determine segment length and direction. Using the exposure length, and the magnitude and orientation of the fitted line segment, the in-plane velocity components were estimated. Pixel groups which were poorly represented by a line segment (evaluated using the normalized residual of the least-squares fit) were rejected as being falsely identified particles. The compiled velocity vectors are presented in Fig. 5. Note that due to the 15 Hz sample frequency used in this experiment, the particles observed in subsequent frames were not related, and thus the particle acceleration could not be determined. Finally, the cameras were unable to provide the necessary resolution to measure the size of the particle—only the re-radiative glow was captured.

With this approach, the velocities are projected in the plane captured by the camera, and they are thus subjected to a two-dimensional approximation. As expected, the velocity around the centerline of the sample appears to be smaller since the velocity component in the z direction is not measured.

Most of the particles were observed near the leading edge of the sample with fewer observed downstream. Given that many downstream particles can be observed in

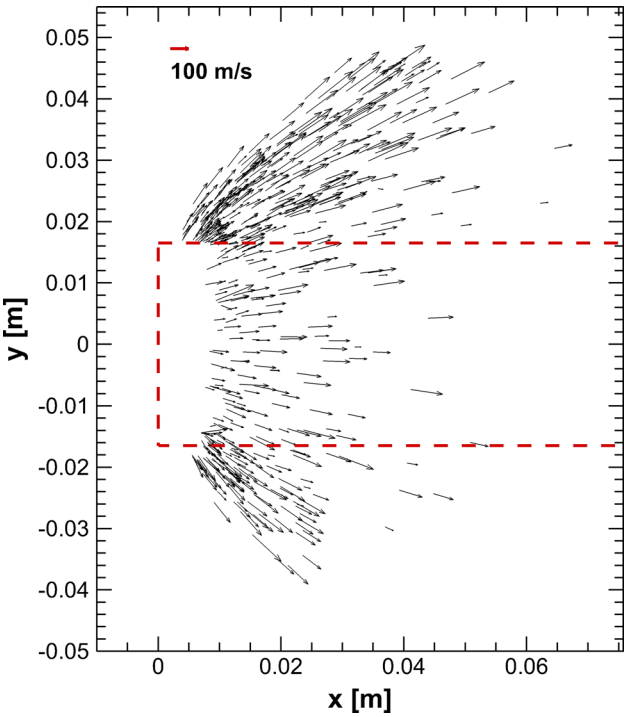

Fig. 5 In-plane velocity vectors of the detected spalled particles estimated by exposure length and pixel grouping geometry. *Red dashed line* shows the location of the sample. *Red reference vector* in *upper left* shows vector length corresponding to 100 m/s

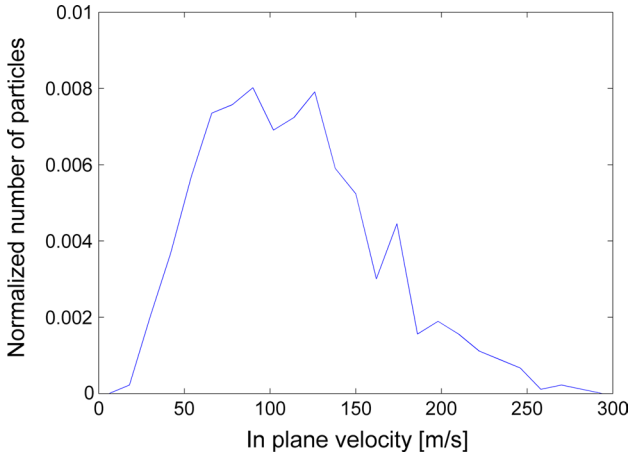

Fig. 6 Probability density function of the in-plane velocity magnitude of detected spalled particles

highly intensified images, it is likely that fewer particles are identified downstream either due to cooling of the particles resulting in less light emission, or due to decomposition of the particles as they traveled downstream. No time-dependent trend was observed in either the number of spalled particles observed or their in-plane velocity. Moreover, particles were observed almost immediately following insertion of the sample into the flow. This suggests that shear plays a significant role in the formation of the particles.

From these results, it is also possible to evaluate the normalized distribution of velocity for all the spalled particles that were identified. Figure 6 plots the distribution of the particle with respect to their calculated *xy*-plane velocity. The probability is calculated by counting the number of particles which have a velocity within a certain range, and then normalizing over the total number of particles. The average velocity component of particles in the two-dimensional image plane was estimated to be 110 m/s, However, the distribution of the particle velocity was skewed, with in-plane velocity magnitudes as high as 300 m/s observed.

4 Conclusions and outlook

This paper presents the recent advances in research related to the ablative phenomenon—spallation. To investigate the effects of spallation on the flow field, a numerical code was developed. The results showed that a spalled particle ejected in a reacting flow would release carbon species in the flow field. This carbon is in sufficient quantity that it is likely to form CN species and, therefore, explain the CN emission detected by spectroscopic experiments.

Short exposure imaging allowed observation of multiple spalled particles during an arcjet test run on PICA and FiberForm® samples.

An automated image analysis procedure allowed positive detection of as many as 722 single particles being ejected from the surface in imagery acquired over the course of a 30-s test of a FiberForm® sample. Visual inspection of the images suggests that many more particles were not positively identified by the procedure.

Particle tracking based on stereoscopic imaging will enable improvements in the determination of particle velocities and trajectories in the three-dimensional space. Using the numerical method combined with the images obtained during the test campaign, it will be possible to gather more information about the trajectory and initial state of the spalled particles. This will lead to a better understanding on how these particles are formed, and what process is responsible for their high-speed ejection.

Acknowledgments Financial support for this work was provided by NASA Award NNX13AN04A, NASA Award NNX14AI97G and NASA Kentucky EPSCoR Award NNX10AV39A. Additional support was generously provided by the Hypersonic EDL program, through M.J. Wright at NASA Ames. The authors are immensely grateful to him. They also would like to thank M.J. Gasch at NASA Ames, as well as J.G. Gragg and S.B. Jones at NASA Langley for their technical assistance. Lastly, the authors are grateful to E. Sozer at NASA Ames for insightful discussions on the CFD code.

References

1. Martin, A., Cozmuta, I., Boyd, I.D., Wright, M.J.: Kinetic rates for gas-Phase chemistry of phenolic-based carbon ablator in atmospheric air. J. Thermophys. Heat Transf. **29**(2), 222 (2015). doi:10.2514/1.T4184
2. Martin, A., Boyd, I.D.: Modeling of heat transfer attenuation by ablative gases during the stardust reentry. J. Thermophys. Heat Transf. **29**(3), 450 (2015). doi:10.2514/1.T4202
3. Weng, H., Bailey, S.C.C., Martin, A.: Numerical study of iso-Q sample geometric effects on charring ablative materials. Int. J. Heat Mass Transf. **80**, 570 (2015). doi:10.1016/j.ijheatmasstransfer.2014.09.040
4. Weng, H., Martin, A.: Multidimensional modeling of pyrolysis gas transport inside charring ablative materials. J. Thermophys. Heat Transf. **28**(4), 583 (2014). doi:10.2514/1.T4434
5. Weng, H., Martin, A.: Numerical investigation of thermal response using orthotropic charring ablative material. J. Thermophys. Heat Transf. **29**(3), 429 (2015). doi:10.2514/1.T4576
6. Miller, M.A., Martin, A., Bailey, S.C.C.: Investigation of the scaling of roughness and blowing effects on turbulent channel flow. Exp. Fluids **55**(2), 1 (2014). doi:10.1007/s00348-014-1675-y
7. Sullivan, J.M., Kobayashi, W.S.: Spallation modeling in the charring material thermal response and ablation (CMA) computer program. In: 22nd AIAA Thermophysics Conference. AIAA Paper 1987–1516, pp. 1–7 (1987). doi:10.2514/6.1987-1516
8. Lundell, J.H.: Spallation of the Galileo probe heat shield. In AIAA/ASME 3rd Joint Thermophysics and Heat Transfer Conference, AIAA Paper 82–0852, St. Louis, MO (1982). doi:10.2514/6.1982-852
9. Wakefield, R.M., Pitts, W.C.: Analysis of the heat-shield experiment on the pioneer-venus entry probes. In: 15th Thermophysics Conference, AIAA Paper 1980–1494, Snowmass, CO (1980). doi:10.2514/6.1980-1494

10. Balakrishnan, A., Nicolet, W.E.: Galileo probe forebody thermal protection - Benchmark heating environment calculations. In: 16th Thermophysics Conference, AIAA Paper 1981–1072, Palo Alto, CA (1981). doi:10.2514/6.1981-1072
11. Milos, F.S.: Galileo probe heat Shield ablation experiment. J. Spacecr. Rockets **34**(6), 705 (1997). doi:10.2514/2.3293
12. Moss, J., Simmonds, A.: Galileo probe forebody flowfield predictions during Jupiter entry. In: 3rd Joint Thermophysics, Fluids, Plasma and Heat Transfer Conference, AIAA Paper 1982–0874, St. Louis, MO (1982). doi:10.2514/6.1982-874
13. Kihara, H., Hatano, M., Nakiyama, N., Abe, K., Nishida, M.: Preliminary studies of spallation particles ejected from an ablator. Trans. Jpn. Soc. Aeronaut. Space Sci. **49**(164), 65 (2006). doi:10.2322/tjsass.49.65
14. Yoshinaka, T.: Spallation measurement at the ablator plasma wind tunnel tests. Tech. Rep. NASDA-TMR-970006E, National Space Development Agency of Japan, Tokyo (1998). https://repository.exst.jaxa.jp/dspace/handle/a-is/31442
15. Davies, C., Park, C.: Trajectories of solid particles spalled from a carbonaceous heat shield. In: 20th Aerospace Sciences Meeting, AIAA Paper 1982-200, Orlando, FL (1982). doi:10.2514/6.1982-200
16. Pace, A., Ruffin, S., Barnhardt, M.: A coupled approach for predicting radiation attenuation in particle-laced flows. In: 42nd AIAA Thermophysics Conference, AIAA Paper 2011-3771, Honolulu, Hawaii (2011). doi:10.2514/6.2011-3771
17. Nozawa, S., Kihara, H., Ichi Abe, K.: Numerical investigation of spalled particle behavior ejected from an ablator surface. Trans. Jpn. Soc. Aeronaut. Space Sci. **8**(ists27), Pe_9 (2010). doi:10.2322/tastj.8.Pe_9
18. Milos, F., Chen, Y.K.: Ablation, thermal response, and chemistry program for analysis of thermal protection systems. In: 10th AIAA/ASME Joint Thermophysics and Heat Transfer Conference, AIAA Paper 2010-4663, Chicago, IL (2010). doi:10.2514/6.2010-4663
19. Inman, J.A., Bathel, B.F., Johansen, C.T., Danehy, P.M., Jones, S.B., Gragg, J.G., Splinter, S.C.: Nitric-Oxide planar laser-induced fluorescence measurements in the hypersonic materials environmental test system. AIAA J. **51**(10), 2365 (2013). doi:10.2514/1.J052246
20. Zhang, H., Weng, H., Martin, A.: Simulation of flow-tube oxidation on the carbon preform of PICA. In 52nd AIAA Aerospace Sciences Meeting, AIAA Paper 2014-1209, National Harbor, MD (2014). doi:10.2514/6.2014-1209
21. Zhang, H., Martin, A., McDonough, J.M.: Parallel efficiency of the freeCFD code for hypersonic flows with chemistry. In: 24th International Conference on Parallel Computational Fluid Dynamics, Atlanta, GA (2012)
22. Park, C.: Assessment of a two-temperature kinetic model for dissociating and weakly ionizing nitrogen. J. Thermophys. Heat Transf. **2**(1), 8 (1988). doi:10.2514/3.55
23. Blottner, F.G., Johnson, M., Ellis, M.: Chemically reacting viscous flow program for multi-component gas mixtures. Tech. Rep. SC-RR-70-754, Sandia National Laboratories, Albuquerque, New Mexico (1971). doi:10.2172/4658539
24. Vincenti, W.G., Kruger, C.H.: Introduction to physical gas dynamics. Krieger Publishing Company, Malabar, Florida (1982)
25. Zhang, H.: High temperature flow solver for aerothermodynamics problems. Ph.D. Thesis, University of Kentucky, Lexington, KY (2015). http://uknowledge.uky.edu/me_etds/64
26. Driver, D.M., MacLean, M.: Improved predictions of PICA recession in arc jet shear tests. In: 49th AIAA Aerospace Sciences Meeting, AIAA Paper 2011-141 (2011). doi:10.2514/6.2011-141
27. Maclean, M., Marschall, J., Driver, D.M.: Finite-Rate surface chemistry model, II: Coupling to viscous navier-stokes code. In: 42nd AIAA Thermophysics Conference, AIAA Paper 2011-3784 (2011). doi:10.2514/6.2011-3784
28. Davuluri, R.S.C., Martin, A.: Numerical study of spallation phenomenon in an arc-jet environment. In: 11th AIAA/ASME Joint Thermophysics and Heat Transfer Conference, AIAA Paper 2014-2249, Atlanta, GA, (2014). doi:10.2514/6.2014-2249
29. Davuluri, R.S.C., Zhang, H., Martin, A.: Numerical study of spallation phenomenon in an arc-jet environment. J. Thermophys. Heat Transf. **30**(1), 32 (2015). doi:10.2514/1.T4586
30. Davuluri, R.S.C.: Modeling of spallation phenomenon in an arc-jet environment. M.Sc. Thesis, University of Kentucky, Lexington, KY (2015). http://uknowledge.uky.edu/me_etds/63
31. Davuluri, R.S.C., Zhang, H., Martin, A.: Effect of spalled particles thermal degradation on a hypersonic flow field environment. In: 54th AIAA Aerospace Sciences Meeting, AIAA Paper 2016-0248, San Diego, CA (2016). doi:10.2514/6.2016-0248
32. Danehy, P.M., Hires, D.V., Johansen, C.T., Bathel, B.F., Jones, S.B., Gragg, J.G., Splinter, S.C.: Quantitative spectral radiance measurements in the HYMETS arc jet. In: 50th AIAA Aerospace Sciences Meeting and Exhibit, AIAA Paper 2012-856, Nashville, TN (2012). doi:10.2514/6.2012-856
33. Majid, A., Bauder, U., Herdrich, G., Fertig, M.: Effect of dust particles on space vehicles entering Mars at hypersonic speeds. In: 63rd International Astronautical Congress (IAC 2012), IAC-12, A3,3C,11, x13315, Naples, Italy (2012). http://iafastro.directory/iac/archive/browse/IAC-12/A3/3C/13315/
34. Majid, A., Bauder, U., Stindl, T., Fertig, M., Herdrich, G., Röser, H.P.: Development of a two phase solver accounting for solid particles in continuum gas flows. In: 40th Thermophysics Conference, AIAA Paper 2008-4105, Seattle, WA (2008). doi:10.2514/6.2008-4105
35. Raiche, G.A., Driver, D.M.: Shock layer optical attenuation and emission spectroscopy measurements during arc jet testing with ablating models. In: 42th AIAA Aerospace Sciences Meeting and Exhibit, AIAA Paper 2004-0825, Reno NV (2004). doi:10.2514/6.2004-825
36. Park, C., Raiche, G.A., Driver, D.M.: Radiation of spalled particles in shock layers. J. Thermophys. Heat Transf. **18**(4), 519 (2004). doi:10.2514/1.8098
37. Tran, H.K., Johnson, C.E., Rasky, D.J., Hui, F.C.L., Hsu, M.T., Chen, Y.K.: Phenolic impregnated carbon ablators (PICA) for discovery class missions. In: 31st AIAA Thermophysics Conference. AIAA Paper 1996-1911, New Orleans, LA, pp. 1–14 (1996). doi:10.2514/6.1996-1911